BIOCHEMISTRY

 Volume 45, Number 7 February 21, 2006

Articles

Prostaglandin $F_{2\alpha}$ Formation from Prostaglandin H_2 by Prostaglandin F Synthase (PGFS): Crystal Structure of PGFS Containing Bimatoprost[†,‡]

Junichi Komoto,[§] Taro Yamada,[§] Kikuko Watanabe,[||] David F. Woodward,[⊥] and Fusao Takusagawa*[,§]

Department of Molecular Biosciences, University of Kansas, 1200 Sunnyside Avenue, Lawrence, Kansas 66045-7534, Division of Applied Life Science, Graduate School of Integrated Science and Art, University of East Asia, 2-1 Ichinomiya-gakuencho, Shimonoseki, Yamaguchi 751-0807, Japan, Department of Biological Sciences, Allergan, Inc., 2525 Dupont Drive (RD-2C), Irvine, California 92612

Received September 13, 2005; Revised Manuscript Received December 23, 2005

ABSTRACT: Prostaglandin H_2 (PGH_2) formed from arachidonic acid is an unstable intermediate and is efficiently converted into more stable arachidonate metabolites by the action of enzymes. Prostaglandin F synthase (PGFS) has dual catalytic activities: formation of $PGF_{2\alpha}$ from PGH_2 by the PGH_2 9,11-endoperoxide reductase activity and 9α,11β-PGF_2 ($PGF_{2\alpha\beta}$) from PGD_2 by the PGD_2 11-ketoreductase activity in the presence of NADPH. Bimatoprost (BMP), which is a highly effective ocular hypotensive agent, is a $PGF_{2\alpha}$ analogue that inhibits both the PGD_2 11-ketoreductase and PGH_2 9,11-endoperoxide reductase activities of PGFS. To examine the catalytic mechanism of PGH_2 9,11-endoperoxide reductase, a crystal structure of PGFS[NADPH + BMP] has been determined at 2.0 Å resolution. BMP binds near the PGD_2 binding site, but the α- and ω-chains of BMP are locate on the ω- and α-chains of PGD_2, respectively. Consequently, the bound BMP and PGD_2 direct their opposite faces of the cyclopentane moieties toward the nicotinamide ring of the bound NADP. The α- and ω-chains of BMP are involved in H-bonding with protein residues, while the cyclopentane moiety is surrounded by water molecules and is not directly attached to either the protein or the bound NADPH, indicating that the cyclopentane moiety is movable in the active site. From the complex structure, two model structures of PGFS containing $PGF_{2\alpha}$ and PGH_2 were built. On the basis of the model structures and inhibition data, a putative catalytic mechanism of PGH_2 9,11-endoperoxide reductase of PGFS is proposed. Formation of $PGF_{2\alpha}$ from PGH_2 most likely involves a direct hydride transfer from the bound NADPH to the endoperoxide of PGH_2 without the participation of specific amino acid residues.

$PGF_{2\alpha}$,[1] one of the earliest discovered and most common prostaglandins, is actively biosynthesized in various organs of mammals (*1*−*7*) and exhibits a variety of biological activities, including contraction of pulmonary arteries (*8*−*11*). $PGF_{2\alpha}$ is mainly synthesized directly from PGH_2 by PGH_2 9,11-endoperoxide reductase (*12*−*15*). A small amount of $PGF_{2\alpha}$ is also produced from PGE_2 by PGE_2 9-ketoreductase (*16*, *17*). A $PGF_{2\alpha\beta}$ epimer has been reported to

[†] The work has been partially supported by Grant 0455454Z (F.T.) from the American Heart Association.

[‡] The atomic coordinates and structure factors have been deposited in the Protein Data Bank (entry 2F38).

* To whom all correspondence should be addressed: Department of Molecular Biosciences, 3004 Haworth Hall, University of Kansas, 1200 Sunnyside Ave., Lawrence, KS 66045-7534. Telephone: (785) 864-4727. Fax: (785) 864-5321. E-mail: xraymain@ku.edu.

[§] University of Kansas.
[||] University of East Asia.
[⊥] Allergan, Inc.

10.1021/bi051861t CCC: $33.50
Published on Web 01/28/2006

Chart 1

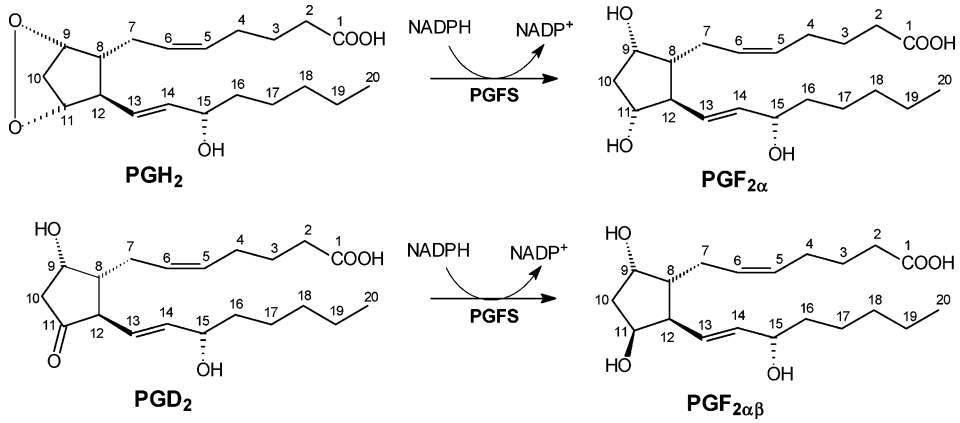

exhibit various biological activities (*18*−*21*), and its levels are increased in bronchoalveolar lavage fluid, plasma, and urine in patients with mastocytosis (*18*) and bronchial asthma (*22*−*24*). $PGF_{2\alpha\beta}$ is synthesized from PGD_2 by PGD_2 11-ketoreductase (*25*, *26*).

PGF synthase (PGFS) was first purified from bovine lung (*15*, *27*). PGFS has dual functions; it catalyzes the formation of $PGF_{2\alpha}$ from PGH_2 by PGH_2 9,11-endoperoxide reductase in the presence of NADPH and also catalyzes the formation of $PGF_{2\alpha\beta}$ from PGD_2 by PGD_2 11-ketoreductase (*28*). However, this enzyme does not catalyze the reduction of PGE_2 (*15*) (Chart 1).

Interestingly, this enzyme exhibits reductase activities toward various carbonyl compounds, such as 9,10-phenanthrenequinone (PQ), *p*-nitrobenzaldehyde, and *p*-nitroacetophenone (*15*). Although the PGD_2 11-ketoreductase activity is competitively inhibited by PQ, the PGH_2 9,11-endoperoxide reductase activity is not inhibited by PQ, suggesting that the PGD_2 and PGH_2 binding sites are different (*15*). PGFS belongs to the aldo-keto reductase family on the basis of its substrate specificity, molecular weight, and amino acid sequence (*29*, *30*). Human 3α-hydroxysteroid dehydrogenase isoforms have been systematically named AKR1C1−AKR1C4, and PGFS, 3α-hydroxysteroid dehydrogenase type 2, is named AKR1C3 (*31*). We proposed a catalytic mechanism for the PGD_2 11-ketoreductase activity of PGFS on the basis of complex structures of PGFS[$NADP^+$ + PGD_2] and PGFS[NADPH + rutin] (*32*), which is similar to the basic mechanism of the aldo-keto reductase family (*33*). Our mechanism uses the catalytic triad (D50···K84···Y55 H-bonding) instead of the catalytic tetrad (D50···K84···Y55···H117 H-bonding) for donation of a proton from Y55 to PGD_2 (*33*). Also, in our mechanism, H117 might act as a general acid at a low pH to donate a proton to PGD_2.

Recent reports suggest that the PGFS activity is high in gastrointestinal tumors, and nonsteroidal anti-inflammatory drugs (NSAIDs) protect against the progression of gastrointestinal tumors (*34*−*40*). There is a growing body of evidence which shows that NSAIDs may also protect against a variety of other cancers, including prostate carcinoma and, most recently, leukemia (*34*−*40*). For example, treatment of leukemia HL-60 cell line cells with indomethacin (IMN) inhibits the growth of HL-60 cells, and overexpression of PGFS in myeloid cells promotes proliferation, suggesting that IMN inhibits PGFS (*41*−*43*). Indeed, a crystal structure of PGFS containing IMN has been determined (*44*). PGFS is inhibited by NSAIDs such as Suprofen (IC_{50} = 0.6 μM), Flurbirofen (IC_{50} = 0.8 μM), Ketoprofen (IC_{50} = 3.8 μM), and IMN (IC_{50} = 4.1 μM) (*45*), and these NSAIDs have preventive activity against the progression of gastrointestinal tumors. Therefore, specific inhibitors of PGFS might be important anticancer drugs.

Recently, it has become apparent that there are neutral lipids of several existing fatty acids (*46*−*55*). These neutral lipids occur in the form of an amide, ether, or ester, which replaces the invariant carboxylic acid moiety. Anandamide and 2-arachidonyl glycerol are examples of neutral lipids that are substrates for cyclooxygenase-2 (COX-2). The resultant products are prostaglandin amides (prostamides) or glyceryl esters (*49*, *51*). Reduction of prostamide produces biologically active prostamide $F_{2\alpha}$. Bimatoprost (BMP) is a synthetic structural analogue of $PGF_{2\alpha}$ in which the charged carboxylic acid group is replaced with a neutral ethylamide substituent.

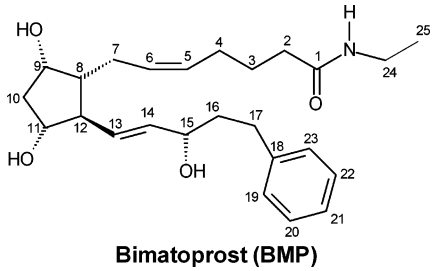

Bimatoprost (BMP)

Structurally, BMP is therefore a prostaglandin amide or prostamide and exhibits biological activity similar to that of prostamide $F_{2\alpha}$ (*56*, *57*). BMP is of particular interest because it is clinically the most efficacious ocular hypotensive agent reported to date, its activity exceeding that of both timolol and latanoprost (*58*, *59*). The ocular hypotensive activity has been suggested to be due to enzymatic hydrolysis to a free acid metabolite that would behave as an authentic prostanoid FP receptor agonist (*60*), but this is controversial (*61*). Also, BMP in-

[1] Abbreviations: AKR, aldo-keto reductase; BMP, bimatoprost; IMN, indomethacin; NADP, either $NADP^+$ or NADPH; NSAIDs, nonsteroidal anti-inflammatory drugs; PGD_2, prostaglandin D_2; $PGF_{2\alpha\beta}$, 9α,11β-prostaglandin F_2; $PGF_{2\alpha}$, 9α,11α-prostaglandin F_2; PGFS, prostaglandin F synthase; PGFS[NADPH + BMP], NADPH- and bimatoprost-bound PGFS; PGFS[NADPH + rutin], NADPH- and rutin-bound PGFS; PGFS[$NADP^+$ + PGD_2], $NADP^+$- and PGD_2-bound PGFS; PGH_2, prostaglandin H_2; PQ, 9,10-phenanthrenequinone.

Table 1: Crystallographic Statistics for PGFS[NADPH + BMP][a]

unit cell dimensions	$a = 44.27$ Å, $b = 78.16$ Å, $c = 48.89$ Å, $\beta = 100.2°$
resolution (Å)	2.0
total no. of observations	117502
no. of unique reflections	19525
completeness (%)	88.7 (63.3)
R_{sym}[b] (outer shell)[c]	0.054 (0.126)
no. of protein non-hydrogen atoms	2563
cofactor	1 NADPH (48 atoms)
substrate/inhibitor	1 BMP (30 atoms)
no. of solvent molecules (H_2O)	109
resolution range (Å)	20−2.0
total no. of reflections used in R_{cryst}	17602
total no. of reflections used in R_{free}	1923
R_{cryst}[d] (outer shell)[c]	0.221 (0.241)
R_{free} (outer shell)[c]	0.281 (0.292)
rmsd for bond distances (Å)	0.007
rmsd for bond angles (deg)	1.2
rmsd for torsion angles (deg)	26
most favored region (%) of the Ramachandran plot	94.0
additional allowed region (%) of the Ramachandran plot	6.0

[a] Space group $P2_1$. The M_r of the subunit is 35 530. The number of complexes in the unit cell is 2. $V_M = 2.34$ Å^3. The percentage of solvent content 47.5%. [b] $R_{sym} = \sum_h \sum_i |I_{hi} - \langle I_h \rangle| / \sum_h \sum_i |I_{hi}|$. [c] Outer shell is 2.0−2.1 Å resolution. [d] $R_{cryst} = \sum_h |F_o - F_c| / \sum_h |F_o|$.

hibits formation of $PGF_{2\alpha}$ from PGH_2 ($IC_{50} = 6\ \mu M$) and formation of $PGF_{2\alpha\beta}$ from PGD_2 ($IC_{50} = 5\ \mu M$) by PGFS (*62*).

Here we describe crystal structures of a human lung PGFS ternary complex, PGFS[NADPH + BMP]. On the basis of the structure, we propose a catalytic mechanism for formation of $PGF_{2\alpha}$ from PGH_2 by PGFS.

EXPERIMENTAL PROCEDURES

Crystallization. Recombinant human lung PGFS was purified from *Escherichia coli* HB101 containing a pUC-hLuFS plasmid encoding the human lung PGFS sequence. The enzyme was purified to electrophoretic homogeneity using methods previously described (*63*). The hanging drop method of vapor diffusion was employed for crystallization of the enzymes. BMP was dissolved in 95% ethanol and added to the crystallization solution just before the crystallization was set up. Thick plate-shaped crystals of PGFS-[NADPH + BMP] suitable for X-ray diffraction studies were grown in a solution containing 1.0 mM BMP, 1.0 mM NADPH, 0.14 M NaCl, 50 mM MES buffer (pH 7.0), and 26% (w/v) PEG 8000 with a protein concentration of 7 mg/mL at 4 °C. The crystals were grown for 14 days.

Data Measurement. The crystal (~0.3 mm × 0.2 mm × 0.1 mm) of PGFS[NADPH + BMP] in a hanging drop was scooped with a nylon loop and dipped into a cryoprotectant solution for 10−15 min, before it was frozen in liquid nitrogen. The cryoprotectant solution was composed of the original mother liquor containing 18% ethylene glycol. The frozen crystal was transferred onto a Rigaku RAXIS IIc imaging plate X-ray diffractometer with a rotating anode X-ray generator as an X-ray source (Cu Kα radiation at 50 kV and 100 mA). The X-ray beam was focused to 0.3 mm by confocal optics (Osmic, Inc.). The diffraction data were measured up to 2.0 Å resolution at −180 °C. The data were processed with DENZO and SCALEPACK (*64*). The statistics are given in Table 1.

Crystal Structure Determination. The unit cell dimensions and space group of the PGFS[NADPH + BMP] crystal indicate that the crystal structure is not isomorphous to that of PGFS[$NADP^+$ + PGD_2]. The crystal structure of the PGFS-[NADPH + BMP] complex was determined by a molecular replacement procedure using the PGFS[$NADP^+$ + PGD_2] structure. The protein structure with the bound NADPH was refined by the simulated annealing procedures of X-PLOR (*65*). The $2F_o - F_c$ and $F_o - F_c$ maps exhibited a large significant residual electron density peak in the active site (Figure 1). A BMP molecule was built into the residual electron density peak. Other well-defined residual peaks were assigned to water molecules. The complex structure and water molecules were refined with all data (no σ cutoff) at 2.0 Å resolution.

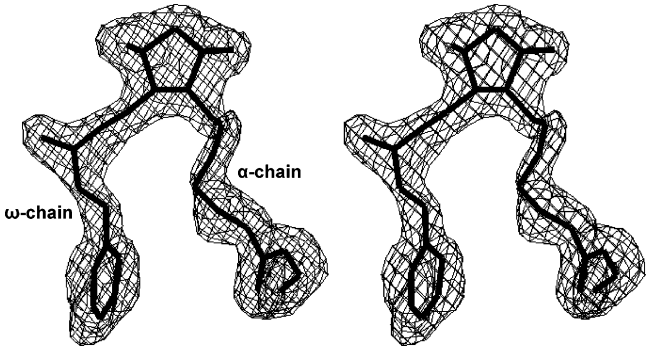

FIGURE 1: $F_o - F_c$ map showing the electron density peak of BMP at a contour level of 2.5σ. The map was calculated after 50 cycles of positional refinement of the final coordinates except for BMP.

Site-Directed Mutagenesis. Oligonucleotide-directed mutagenesis was used to prepare cDNAs encoding the mutated Y55F form of the enzyme (*30*). Mutagenic oligonucleotides was purchased from Integrated DNA Technologies (Coralville, IA). Mutagenesis was performed by the method of Kunkel et al. (*66*), with a Mutan-K site-directed mutagenesis kit (Takara Shuzo, Kyoto, Japan). A clone containing the Y55F mutation was identified by nucleotide sequence analysis across the mutation site by the dideoxy chain termination method (*67*).

PGD_2 11-Ketoreductase Activity ($PGD_2 \rightarrow PGF_{2\alpha\beta}$) Assay. The PGD_2 11-ketoreductase activity and the PGH_2 9,11-endoperoxide reductase activity of the Y55F mutated enzyme were measured as described previously (*15*). The standard reaction mixture that contains 100 mM potassium phosphate buffer (pH 6.5), 500 μM NADPH, and 1.5 mM [^{3}H]PGD_2 (0.14 μCi) was prepared. The reaction was initiated by adding 10 μL of the enzyme (1 mg/mL) to 90 μL of the standard reaction mixture, and the mixture was incubated at 37 °C for 30 min. Blanks contained the reaction mixture without the enzyme. The reaction was stopped by the addition of 250 μL of a cold diethyl ether/methanol/200 mM citric acid mixture (30:4:1), and PGs were extracted into the organic phase. The mixture of PGD_2 and $PGF_{2\alpha\beta}$ (20 μg each) was added to the solution as authentic markers. The organic phase (150 μL) was subjected to thin-layer chromatography in a diethyl ether/methanol/acetic acid solvent system (90:2:0.1). The positions of the PGs on the silica gel plate were visualized with iodine vapor. Silica gel was scraped off in sections corresponding to PGD_2, $PGF_{2\alpha\beta}$, and others, and the radioactivity of each section was measured by a liquid scintillation spectrometer in a toluene solution containing 0.01% 1,4-bis[2-(4-methyl-5-phenyloxazolyl)]benzene and 0.5% 2,5-diphenyloxazole.

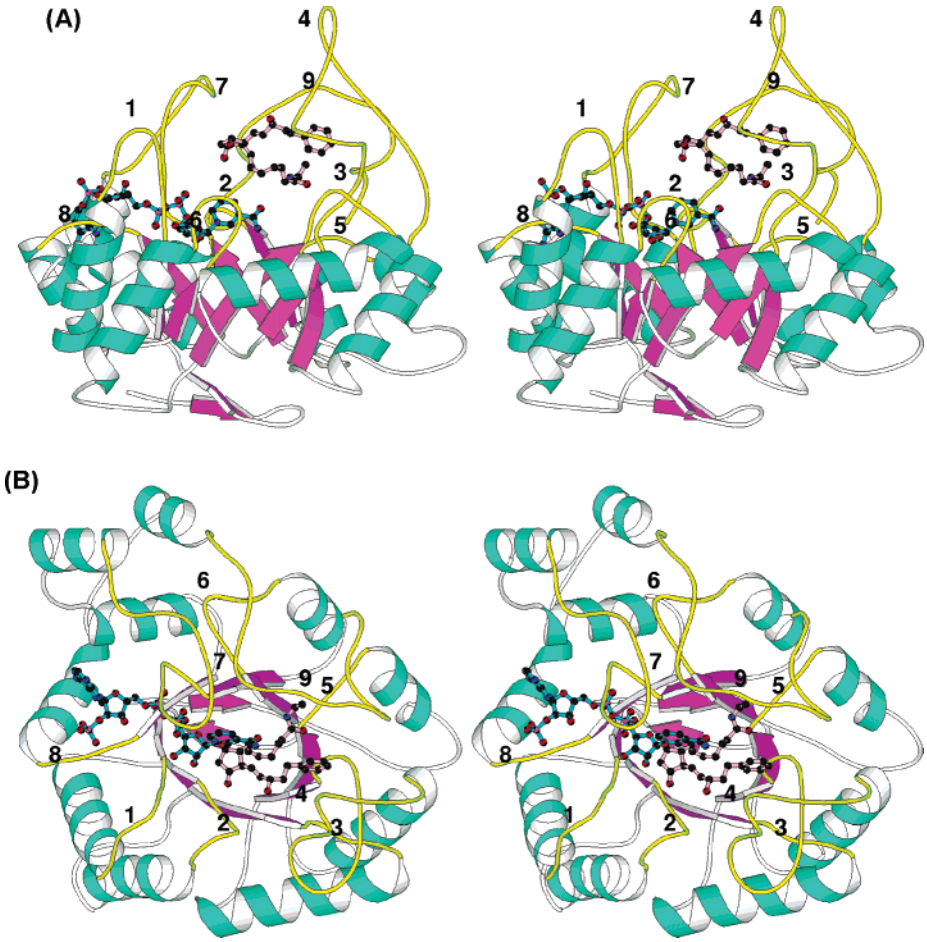

FIGURE 2: Ribbon drawings of PGFS[NADPH + BMP]: (A) side view and (B) top view. The α-helices and β-strands in the α/β-base are colored aquamarine and magenta, respectively. The loops are colored yellow with numbers. The bound NADPH and BMP are colored cyan and light pink, respectively. The topology of the polypeptide is ~B1(7−9)-B2(15−17)-β1(19−22)-(loop 1)-α1(32−44)-β2(48−50)-(loop 2)-α2(58−70)-β3(80−85)-(loop 3)-α3(92−106)-β4(113−116)-(loop 4)-α4(144−156)-β5(162−166)-(loop 5)-α5(170−177)-β6(188−192)-(loop 6)-α6(200−208)-β7(212−216)-(loop 7)-α7(239−248)-H1(252−262)-β8(266−270)-(loop 8)-α8(274−284)-H2(290−297)-(loop 9). B1 and B2 are extra β-strands that are not involved in the β-barrel structure component.

PGH_2 9,11-Endoperoxide Reductase Activity ($PGH_2 \rightarrow PGF_{2\alpha}$) Assay. The PGH_2 9,11-endoperoxide reductase activity was assayed under the same conditions that were used for the PGD_2 11-ketoreductase activity except that 80 μM [1-^{14}C]PGH_2 (0.1 μCi) was used as a substrate in place of 1.5 mM [^{3}H]PGD_2 and that the incubation time was 1 min at 30 °C.

RESULTS AND DISCUSSION

Overall Structure. The crystallographic refinement parameters (Table 1), final $2F_o - F_c$ maps, and conformational analysis by PROCHECK (*68*) indicate that the crystal structure of the PGFS[NADPH + BMP] complex has been determined with acceptable statistics. As shown in Figure 2, the protein structure of PGFS displays the characteristic fold of the AKR superfamily (*69*), an $(\alpha/\beta)_8$ barrel with three associated large loops. The β-strands (β1−β8) form the cylindrical core of the barrel and are surrounded by α-helices (α1−α8), while the accompanying loops (loop 4, loop 7, and loop 9) partially cover the C-terminal end of the barrel. In addition to the $(\alpha/\beta)_8$ core structure, there are two β-strands (B1 and B2) from the N-terminus sealing the N-terminal end of the barrel and two α-helices (H1 and H2) from the C-terminal part of the molecule packed by the side of the barrel. These additional β-strands and α-helices are conserved in other AKR structures (*69*).

Cofactor (NADPH) binds in a deep cavity at the C-terminal end of the barrel and extends across the barrel closer to the core. The bound NADPH is heavily involved in H-bonds with amino acid residues in the loops connecting β-strands and α-helices. The nicotinamide moiety is located within the enzyme near the center of the barrel, while the adenine moiety is exposed on the outer surface of the protein.

BMP in the Active Site. As shown in Figure 3, a BMP molecule is located above the bound NADPH and is surrounded by loop 1, 2, 4, 7, and 9. Although the two hydroxyl groups (O_9 and O_{11}) of the cyclopentane moiety are pointed to the nicotinamide ring of the bound NADPH, there is no significant interaction between them. Each of the O_9 and O_{11} hydroxyl groups of the cyclopentane moiety is involved in two H-bonds with two water molecules (w_2 and w_3, and w_4 and w_5, respectively). The ethylamide α-chain is deep within the active site cavity, while the phenyl ω-chain is located above the α-chain. O_1 and $N_{1'}$ in the α-chain participate in H-bonds with O_G of S118 and w_1, respectively. Although O_H of Y319 can be near $N_{1'}$ to form a H-bond, there is no H-bond between them because of the presence of the ethyl moiety. The hydroxyl group O_{15} in the ω-chain

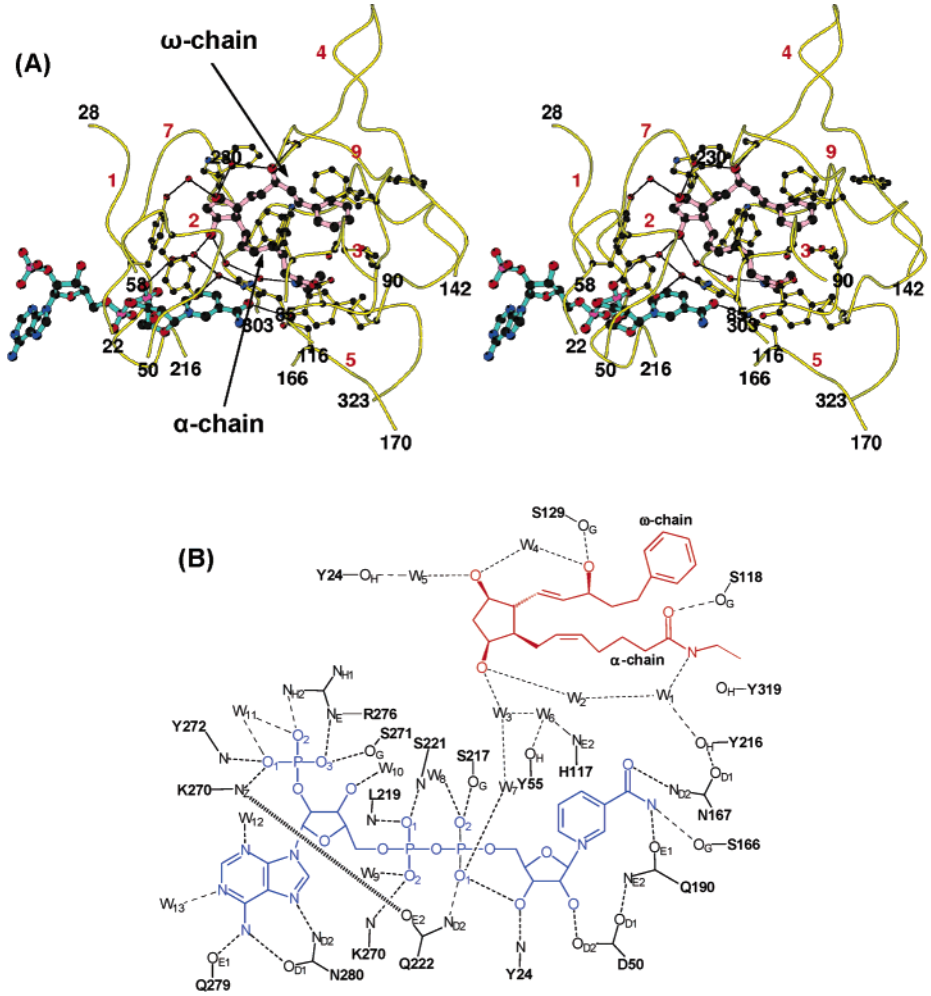

FIGURE 3: (A) Active site geometry. Thin lines illustrate possible H-bonds among NADPH (aquamarine), BMP (magenta), and loop structures (yellow). (B) Schematic illustration showing possible H-bonds in the active site of PGFS[NADPH + BMP]. W's represent water molecules. A thick dashed line indicates a "safety belt" hydrogen bond.

participates in a H-bond with O_G of S129 and w_4. Therefore, the polar groups of α- and *ω*-chains (tails) are directly connected to the protein with H-bonds, while the cyclopentane moiety (head) is associated with water molecules, suggesting that the cyclopentane moiety is movable in the active site cavity. Although the polar groups of BMP are involved in H-bonds, BMP is bound to the protein by mainly hydrophobic interactions. There are seven aromatic residues (Y24, W86, F139, W227, F306, F311, and Y319) surrounding the bound BMP. W227 is located over the cyclopentane moiety of BMP as if it seals the bound BMP into the active site cavity.

Since BMP is an analogue of $PGF_{2\alpha}$, a $PGF_{2\alpha}$ molecule can be completely superimposed on the bound BMP and forms the same H-bonds that were observed for BMP, except that $O_{1'}$ of the carboxyl group forms a H-bond with O_H of Y319 and water (w_1). This modeling suggests that the product $PGF_{2\alpha}$ from PGH_2 might bind to the same site as BMP before being released from the active site cavity. An inhibition study supports this conclusion because BMP inhibits the 9,11-endoperoxide reductase activity as well as the 11-ketoreductase activity of PGFS (*62*).

A Comparison of the PGD_2 and BMP Binding Sites. Although the crystal structure of PGFS[NADPH + BMP] is not isomorphous to that of PGFS[$NADP^+$ + PGD_2], the peptide fold is identical within experimental error. Significant movements are only observed in the side chains of W227 and F311. These aromatic residues are two of seven residues surrounding BMP, suggesting that the PGFS structure is relatively rigid. The $NADP^+$ and NADPH binding sites in the PGFS structure are the same within experimental error (rmsd = 0.22 Å), and their H-bonding networks are also the same. Although PGD_2 and BMP bind to a similar site, there are several significant differences between their binding schemes. The α- and *ω*-chains of BMP are located on the *ω*- and α-chains of PGD_2, respectively, indicating that the BMP and PGD_2 binding schemes are flipped. The bound BMP and PGD_2 direct their opposite faces of the cyclopentane moieties toward the nicotinamide ring of the bound NADP (Figure 4).

PGFS has an oxyanion hole in the active site. In the PGFS-[$NADP^+$ + PGD_2] structure, the carbonyl oxygen (O_{11}) of PGD_2 is pulled into the oxyanion hole and forms H-bonds with O_H of Y55 and N_{E2} of H117. On the other hand, no part of BMP is near the oxyanion hole in the PGFS[NADPH + BMP] structure. A water (w_6) is located in the oxyanion hole and forms H-bonds with Y55 and H117. Consequently, the positions of the cyclopentane moieties of BMP and PGD_2 are significantly different, suggesting that the catalytic sites of 11-ketoreductase and 9,11-endoperoxide reductase in PGFS are in different locations in the active site cavity.

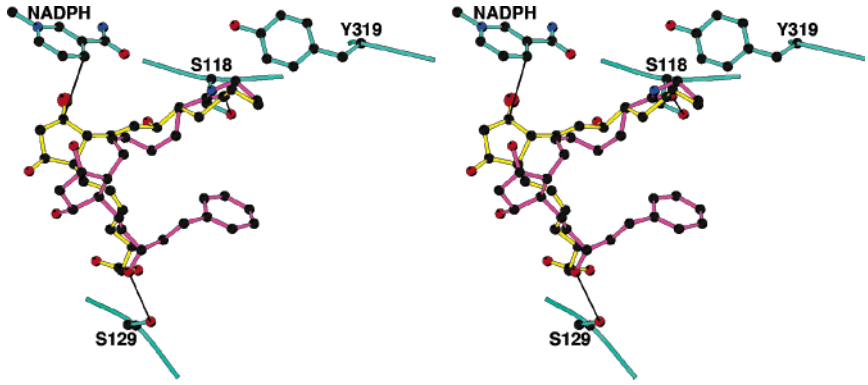

FIGURE 4: Superimposed view of BMP (magenta) in the PGFS[NADPH + BMP] structure and PGD_2 (yellow) in the PGFS[$NADP^+$ + PGD_2] structure showing that both molecules approximately overlap. However, the bound BMP and PGD_2 direct their opposite faces of the cyclopentane moieties toward the nicotinamide ring of the bound NADP. O_{11} of PGD_2 which is in an oxyanion hole is depicted as a larger red sphere. Thin lines denote possible H-bonds between BMP and PGFS. Direct hydride transfer that would occur between C_{11} of PGD_2 and C_4 of $NADP^+$ is shown as a thin line.

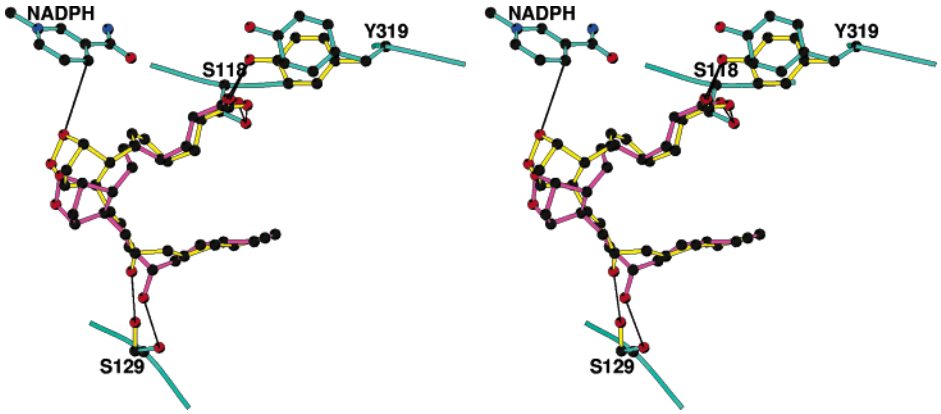

FIGURE 5: Model structure of PGFS[NADPH + PGH_2] built based on the PGFS[NADPH + BMP] structure. The bound BMP is converted to $PGF_{2\alpha}$ by replacing the ethyl amide group with oxygen and modifying the phenyl group to the tail of the ω-chain. PGH_2 (magenta) is built from the resultant $PGF_{2\alpha}$ by forming the endoperoxide. A swinging model (yellow) is built as follows. The cyclopentane moiety is swung toward the bound NADPH so that O_9 is sufficiently close to receive the *pro-R* hydrogen from C_4 of NADPH. Although the α- and ω-chains were moved slightly, all H-bonds between PGH_2 and PGFS remained.

A Possible Catalytic Mechanism. BMP inhibits the PGD_2 11-ketoreductase activity as well as the PGH_2 9,11-endoperoxide reductase activity (*62*). From the crystal structures of PGFS[$NADP^+$ + PGD_2] and PGFS[NADPH + BMP], the PGD_2 11-ketoreductase inhibitory activity of BMP is quite obvious because the two molecules bind to a similar region in the active site cavity. Since BMP is a $PGF_{2\alpha}$ analogue and also inhibits the PGH_2 9,11-endoperoxide reductase reaction, it is reasonable to assume that PGH_2 and $PGF_{2\alpha}$ bind to the BMP binding site. On the basis of this assumption, we can build a model structure of PGFS[$NADP^+$ + $PGF_{2\alpha}$] from PGFS[NADPH + BMP] and another model structure of PGFS[NADPH + PGH_2] by forming the endoperoxide between O_9 and O_{11} (Figure 5). The endoperoxide moiety of PGH_2 in the model structure is too distant to transfer a hydride directly from the bound NADPH. In PGFS[NADPH + BMP], the cyclopentane moiety of BMP is surrounded by water molecules (w_2−w_5) and does not directly attach to the protein through H-bonding, suggesting that the cyclopentane moiety is movable in the active site cavity. As shown in Figure 5, the cyclopentane moiety of BMP can be moved toward the bound NADPH without breaking the H-bonds between the chains of PGH_2 and the protein. In this model structure, O_9 of PGH_2 is brought near the bound NADPH and is able to receive the *pro-R* hydrogen from the bound NADPH.

On the basis of these two PGFS[NADPH + PGH_2] model structures, we propose a putative catalytic mechanism for the $PGH_2 \rightarrow PGF_{2\alpha}$ reaction. PGH_2 binds at the BMP binding site found in the crystal structure (model 1, colored magenta in Figure 5), and the cyclopentane−endoperoxide moiety swings toward the bound NADPH (model 2, colored yellow in Figure 5) without breaking the H-bonds of the α- and ω-chains. In this geometry, O_9 of PGH_2 can be located within 3.5 Å of C_4 of NADPH, the *pro-R* hydrogen of NADPH can be directly transferred to O_9 of PGH_2, and the O_9−O_{11} bond is broken in a concerted fashion (Figure 6A). The negatively charged O_{11} receives a proton from the solution to complete the reaction, and the resulting $PGF_{2\alpha}$ is released from the active site cavity. The proposed catalysis occurs only if the endoperoxide moiety of PGH_2 is oriented correctly relative to the bound NADPH, whose location and orientation did not vary in the three crystal structures (PGFS[$NADP^+$ + PGD_2], PGFS[NADPH + rutin], and PGFS[NADPH + BMP]).

Obviously, the proposed mechanism for formation of $PGF_{2\alpha}$ from PGH_2 is different from that of formation of $PGF_{2\alpha\beta}$ from PGD_2 proposed on the basis of PGFS[$NADP^+$ + PGD_2] and PGFS[NADPH + rutin] structures (*32*). In $PGF_{2\alpha\beta}$ formation, a PGD_2 binds to the active site, carbonyl oxygen O_{11} is in the oxyanion hole, and the carbonyl carbon (C_{11}) directs its *re* face toward the nicotinamide ring of the

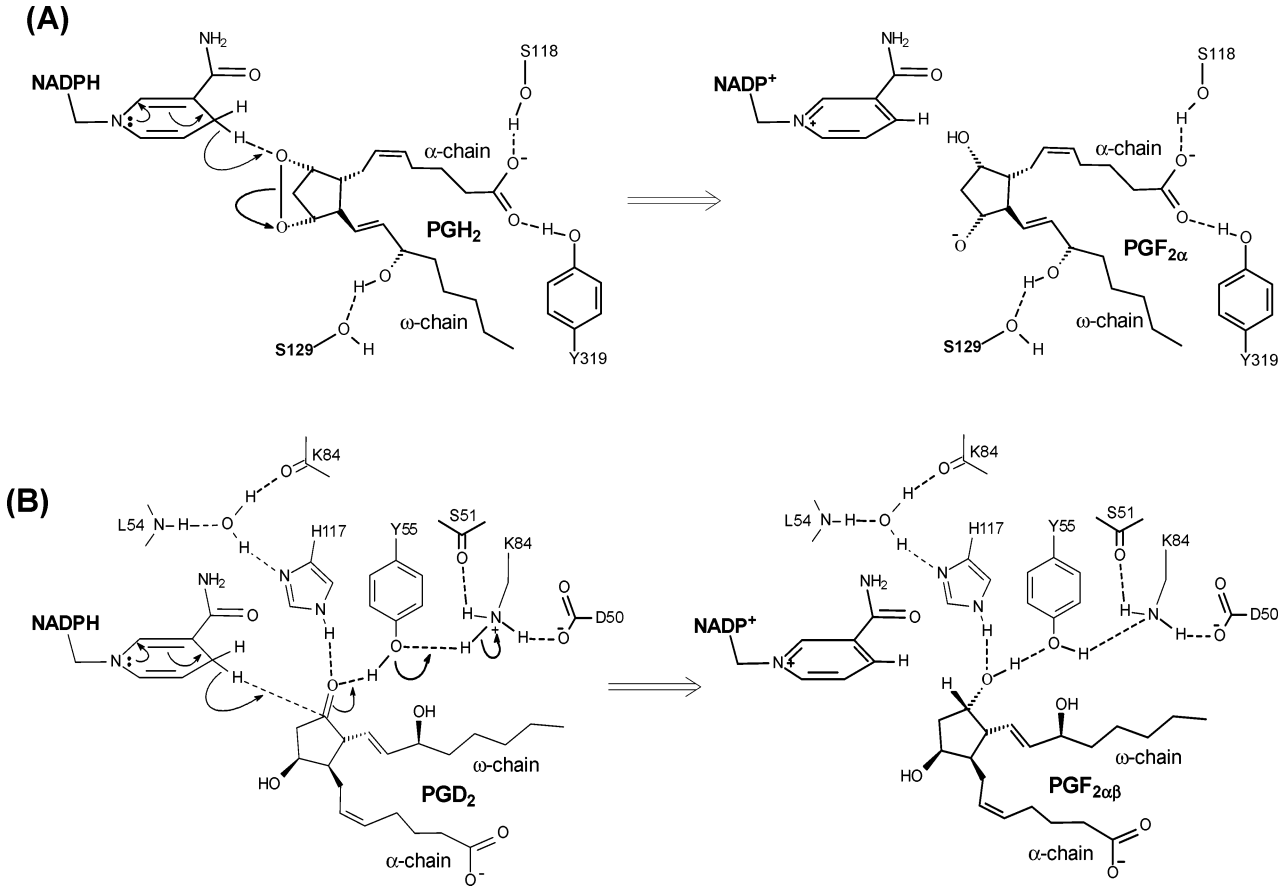

FIGURE 6: Catalytic mechanisms of PGFS proposed on the basis of the crystal structures of PGFS[NADPH + BMP] and PGFS[$NADP^+$ + PGD_2]. (A) PGH_2 9,11-endoperoxide reductase. A PGH_2 binds to the active site, and the polar groups of the α- and *ω*-chains form H-bonds with PGFS. O_9 of the cyclopentane moiety is brought near the bound NADPH by a swinging motion and receives directly the *pro-R* hydrogen from NADPH. The O_9-O_{11} bond is broken in a concerted fashion. The negatively charged O_{11} receives a proton from the solution to complete the reaction, and a $PGF_{2\alpha}$ is formed. (B) PGD_2 11-ketoreductase. A PGD_2 binds to the active site; carbonyl oxygen O_{11} is in the oxyanion hole, and the carbonyl carbon (C_{11}) directs its *re*-face toward the nicotinamide ring of the bound NADPH. Y55 (or H119) donates a proton to O_{11} of PGD_2, and the *pro-R* hydrogen of NADPH is transferred directly to C_{11} of PGD_2 to form $PGF_{2\alpha\beta}$.

bound NADPH. Y55 (or H119) donates a proton to O_{11} of PGD_2, and the *pro-R* hydrogen of NADPH is transferred directly to C_{11} of PGD_2 to form $PGF_{2\alpha\beta}$ (Figure 6B).

Y55 is the essential amino acid residue for the PGD_2 11-ketoreductase activity, while it does not participate in the proposed PGH_2 9,11-endoperoxide reductase activity. Therefore, the Y55F mutated enzyme was prepared, and the PGD_2 11-ketoreductase and PGH_2 9,11-endoperoxide reductase activities were measured. The Y55F mutated enzyme loses the PGD_2 11-ketoreductase activity but retains the PGH_2 9,-11-endoperoxide reductase activity, indicating that the formation of $PGF_{2\alpha\beta}$ from PGD_2 and the formation of $PGF_{2\alpha}$ from PGH_2 utilize the different catalytic mechanism.

Since no specific amino acid residue directly facilitates the hydride transfer in the proposed catalytic mechanism of PGH_2 9,11-endoperoxide reductase, the hydride transfer rate would be slower than that of the PGD_2 11-ketoreductase reaction facilitated by a general acid catalysis. Indeed, the catalytic rate ($k_{cat} = 5.7 \times 10^{-3}\ s^{-1}$) and efficiency ($k_{cat}/K_M = 2.28 \times 10^2\ M^{-1}\ s^{-1}$) of PGH_2 9,11-endoperoxide reductase are lower than those of PGD_2 11-ketoreductase ($k_{cat} = 1.42 \times 10^{-2}\ s^{-1}$, $k_{cat}/K_M = 9.47 \times 10^3\ M^{-1}\ s^{-1}$) (*30*).

$PGF_{2\alpha}$ Binding Site and Mode. The proposed catalytic mechanism assumes that $PGF_{2\alpha}$ binds to the BMP binding site in the same binding mode which is different (flipped mode) from that of PGD_2 found in the crystal structure of PGFS[$NADP^+$ + PGD_2]. It is possible that the bulky ethylamide and phenyl groups at the α- and *ω*-chains, respectively, might prevent the cyclopentane moiety of BMP from entering deeply into the active site cavity as observed in PGD_2 binding and induce BMP to have a mode flipped compared to the PGD_2 binding mode. To examine this possibility, the following three model structures were built: (1) BMP bound to the BMP binding site in the same mode as PGD_2, (2) BMP bound to the PGD_2 binding site in the same mode as PGD_2, and (3) BMP bound to the PGD_2 binding site in the same mode as BMP (flipped mode).

Model 1 was built by flipping the bound BMP, and the conformations of α- and *ω*-chains were varied to superimpose the α- and *ω*-chains on the *ω*- and α-chains of the bound BMP, respectively. Note that O_{11} is far from the oxyanion hole (the bound water w_6 position). Models 2 and 3 were built by placing O_{11} and O_9 of BMP, respectively, in the oxyanion hole; each BMP model structure was rotated at O_{11} or O_9, and the conformations of α- and *ω*-chains were varied to superimpose them on the bound PGD_2 in the PGFS-[$NADP^+$ + PGD_2] structure. Since the active site cavity of PGFS is relatively large, BMP fits well in the active site

cavity in the three model structures without short contacts. Thus, the modeling studies suggest that the BMP binding site and mode found in the PGFS[NADPH + BMP] structure would not be due to the bulky groups attached to the α- and ω-chains.

Since BMP and $PGF_{2\alpha}$ are structurally very similar, $PGF_{2\alpha}$ could bind to PGFS in a manner similar to that of BMP in the model structures; i.e., it could bind to two different sites (PGD_2 and BMP binding sites) in two different binding modes (PGD_2 and flipped modes). However, PGFS does not catalyze the reduction reaction from PGD_2 to $PGF_{2\alpha}$ or from PGE_2 to $PGF_{2\alpha}$ (*28*). Both PGD_2 and PGE_2 are structurally quite similar and have a carbonyl group. One of the characteristic structural features of PGFS is the presence of an oxyanion hole in the active site of 11-ketoreductase. The carbonyl oxygen (O_{11}) of PGD_2 is placed in the oxyanion hole in the PGFS[$NADP^+$ + PGD_2] structure, and thus, the carbonyl group is reduced to a hydroxyl group to produce 9α,11β-PGF_2 ($PGF_{2\alpha\beta}$) but not 9α,11α-PGF_2 ($PGF_{2\alpha}$). On the other hand, if PGE_2 were to bind to the PGD_2 binding site in the flipped mode to place carbonyl O_9 in the oxyanion hole, the carbonyl group (C_9═O_9) would be reduced to $PGF_{2\alpha}$. However, PGE_2 is not reduced to $PGF_{2\alpha}$ by PGFS, indicating that PGE_2 and $PGF_{2\alpha}$ do not bind to the PGD_2 binding site in the flipped mode. Therefore, the catalytic activity of PGFS indicates that the "real" $PGF_{2\alpha}$ binding site must be shifted from the PGD_2 binding site (i.e., O_9 or O_{11} is not in the oxyanion hole) and thus eliminates the model 2 and 3 structures. Although the cyclopentane moiety of BMP ($PGF_{2\alpha}$) in model 1 is shifted from that of PGD_2, O_9 and O_{11} are not pointed toward the nicotinamide ring of the bound NADPH, suggesting that the model 1 structure is not suitable for $PGF_{2\alpha}$ production. Since the BMP binding site found in the PGFS[NADPH + BMP] structure is shifted from that of PGD_2 but O_9 is near C_4 of the nicotinamide ring of the bound NADPH, it is reasonable to conclude that $PGF_{2\alpha}$ and BMP bind to the same site in the same mode (flipped mode).

ACKNOWLEDGMENT

We express our thanks to Professor Richard H. Himes for a critical reading of the manuscript and very valuable comments.

REFERENCES

1. Gerozissis, K., Saavedra, J. M., and Dray, F. (1983) Prostanoid profile in specific brain areas, pituitary and pineal gland of the male rat. Influence of experimental conditions, *Brain Res. 279*, 133−139.
2. Ogorochi, T., Narumiya, S., Mizuno, N., Yamashita, K., Miyazaki, H., and Hayaishi, O. (1984) Regional distribution of prostaglandins D_2, E_2, and $F_{2\alpha}$ and related enzymes in postmortem human brain, *J. Neurochem. 43*, 71−82.
3. Ujihara, M., Urade, Y., Eguchi, N., Hayashi, H., Ikai, K., and Hayaishi, O. (1988) Prostaglandin D_2 formation and characterization of its synthetases in various tissues of adult rats, *Arch. Biochem. Biophys. 260*, 521−531.
4. Seregi, A., Forstermann, U., Heldt, R., and Hertting, G. (1985) The formation and regional distribution of prostaglandins D_2 and $F_{2\alpha}$ in the brain of spontaneously convulsing gerbils, *Brain Res. 337*, 171−174.
5. Hayashi, H., Ito, S., Tanaka, T., Negishi, M., Kawabe, H., Yokohama, H., Watanabe, K., and Hayaishi, O. (1987) Determination of 9α,11β-prostaglandin F_2 by stereospecific antibody in various rat tissues, *Prostaglandins 33*, 517−530.
6. Bergström, S. (1966) in *Nobel Symposum 2, Prostaglandins* (Bergström, S., and Samuelsson, B., Eds.) pp 21−30, Almqvist and Wiksell, Stockholm.
7. Karim, S. M., Sandler, M., and Williams, E. D. (1967) Distribution of prostaglandins in human tissues, *Br. J. Pharmaol. Chemother. 31*, 340−344.
8. Embrey, M. P., and Morrison, D. L. (1968) The effect of prostaglandins on human pregnant myometrium *in vitro*, *J. Obstet. Gynaecol. Br. Commonw. 75*, 829−832.
9. Karim, S. M., Trussell, R. R., Patel, R. C. and Hillier, K. (1968) Response of pregnant human uterus to prostaglandin-F_2-α-induction of labour, *Br. Med. J. 4*, 621−623.
10. Hyman, A. L. (1969) The active responses of pulmonary veins in intact dogs to prostaglandins $F_{2\alpha}$ and E_1, *J. Pharmacol. Exp. Ther. 165*, 267−273.
11. Mathé, A. A. (1977) in *The Prostaglandins* (Ramwell, P. W., Ed.) Vol. 3, pp 169−224, Plenum, New York.
12. Hamberg, M., and Samuelsson, B. (1967) On the mechanism of the biosynthesis of prostaglandins E-1 and F-1-α, *J. Biol. Chem. 242*, 5336−5343.
13. Wlodawer, P., Kindahl, H., and Hamberg, M. (1976) Biosynthesis of prostaglandin $F_{2\alpha}$ from arachidonic acid and prostaglandin endoperoxides in the uterus, *Biochim. Biophys. Acta 431*, 603−614.
14. Qureshi, Z., and Cagen, L. M. (1982) Prostaglandins $F_{2\alpha}$ produced by rabbit renal slices is not a metabolite of prostaglandins E_2, *Biochem. Biophys. Res. Commun. 104*, 1255−1263.
15. Watanabe, K., Yoshida, R., Shimizu, T., and Hayaishi, O. (1985) Enzymatic formation of prostaglandin $F_{2\alpha}$ from prostaglandin H_2 and D_2. Purification and properties of prostaglandin F synthetase from bovine lung, *J. Biol. Chem. 260*, 7035−7041.
16. Leslie, C. A., and Levine, L. (1973) Evidence for the presence of a prostaglandin E 2-9-keto reductase in rat organs, *Biochem. Biophys. Res. Commun. 52*, 717−724.
17. Lin, Y.-M., and Jarabak, J. (1978) Isolation of two proteins with 9-ketoprostaglandin reductase and NADP-linked 15-hydroxyprostaglandin dehydrogenase activities and studies on their inhibition, *Biochem. Biophys. Res. Commun. 81*, 1227−1234.
18. Liston, T. E., and Roberts, L. J., II (1985) Transformation of prostaglandin D_2 to 9α,11β-(15S)-trihydroxyprosta-(5Z,13E)-dien-1-oic acid (9α,11β-prostaglandin F_2): A unique biologically active prostaglandin produced enzymatically *in vivo* in humans, *Proc. Natl. Acad. Sci. U.S.A. 82*, 6030−6034.
19. Pugliese, G., Spokas, E. G., Marcinkiewicz, E., and Wong, P. Y.-K. (1985) Hepatic transformation of prostaglandin D_2 to a new prostanoid, 9α,11β-prostaglandin F_2, that inhibits platelet aggregation and constricts blood vessels, *J. Biol. Chem. 260*, 14621−14625.
20. Beasley, C. R., Robinson, C., Featherstone, R. L., Varley, J. G., Hardy, C. C., Church, M. K., and Holgate, S. T. (1987) 9α,11β-Prostaglandin F_2, a novel metabolite of prostaglandin D_2 is a potent contractile agonist of human and guinea pig airways, *J. Clin. Invest. 79*, 978−983.
21. Seibert, K., Sheller, J. R., and Roberts, L. J., II (1987) (5Z,13E)-(15S)-9α,11β,15-trihydroxyprosta-5,13-dien-1-oic acid (9α,11β-prostaglandin F_2): Formation and metabolism by human lung and contractile effects on human bronchial smooth muscle, *Proc. Natl. Acad. Sci. U.S.A. 84*, 256−260.
22. Dworski, R., Fitzgerald, G. A., Oates, J. A., and Sheller, J. R. (1994) Effect of oral prednisone on airway inflammatory mediators in atopic asthma, *Am. J. Respir. Crit. Care Med. 149*, 953−959.
23. Obata, T., Nagakura, T., Kammuri, M., Masaki, T., Maekawa, K., and Yamashita, K. (1994) Determination of 9α,11β-prostaglandin F_2 in human urine and plasma by gas chromatography−mass spectrometry, *J. Chromatogr., Biomed. Appl. 655*, 173−178.
24. O'Sullivan, S., Dahlén, B., Dahlén, S. E., and Kumlin, M. (1996) Increased urinary excretion of the prostaglandin D_2 metabolite 9α,-11β-prostaglandin F_2 after aspirin challenge supports mast cell activation in aspirin-induced airway obstruction, *J. Allergy Clin. Immunol. 98*, 421−432.
25. Watanabe, K., Shimizu, T., and Hayaishi, O. (1981) Enzymatic conversion of prostaglandin D_2 to $F_{2\alpha}$ in the rat lung, *Biochem. Int. 2*, 603−610.
26. Wong, P. Y.-K. (1981) Purification and partial characterization of prostaglandin D_2 11-keto reductase in rabbit liver, *Biochim. Biophys. Acta 659*, 169−178.

27. Chen, L.-Y., Watanabe, K., and Hayaishi, O. (1992) Purification and characterization of prostaglandin F synthase from bovine liver, *Arch. Biochem. Biophys. 296*, 17−26.
28. Watanabe, K., Iguchi, Y., Iguchi, S., Arai, Y., Hayaishi, O., and Roberts, L. J., II (1986) Stereospecific conversion of prostaglandin D_2 to (5Z,13E)-(15S)-9α-11β,15-trihydroxyprosta-5,13-dien-1-oic acid (9α,11β-prostaglandin F_2) and of prostaglandin H_2 to prostaglandin $F_{2\alpha}$ by bovine lung prostaglandin F synthase, *Proc. Natl. Acad. Sci. U.S.A. 83*, 1583−1587.
29. Watanabe, K., Fujii, Y., Nakayama, K., Ohkubo, H., Kuramitsu, S., Kagamiyama, H., Nakanishi, S., and Hayaishi, O. (1988) Structural Similarity of Bovine Lung Prostaglandin F Synthase with ϵ-Crystallin of European Common Frog, *Proc. Natl. Acad. Sci. U.S.A. 85*, 11−15.
30. Suzuki, K., Fujii, Y., Miyano, M., Chen, L.-Y., Takahashi, T., and Watanabe, K. (1999) cDNA Cloning, Expression, and Mutagenesis Study of Liver-type Prostaglandin F Synthase, *J. Biol. Chem. 274*, 241−248.
31. Jez, J. M., Flynn, T. G., and Penning, T. M. (1997) A new nomenclature for the aldo-keto reductase superfamily, *Biochem. Pharmacol. 54*, 639−647.
32. Komoto, J., Yamada, T., Watanabe, K., and Takusagawa, F. (2004) Crystal structure of human prostaglandin F synthase (AKR1C3), *Biochemistry 43*, 2188−2198.
33. Schlegel, B. P., Jez, J. M., and Penning, T. M. (1998) Mutagenesis of 3α-hydroxysteroid dehydrogenase reveals a "push-pull" mechanism for proton transfer in aldo-keto reductases, *Biochemistry 37*, 3538−3548.
34. Xu, X. C. (2002) COX-2 inhibitors in cancer treatment and prevention, a recent development, *Anticancer Drugs 13*, 127−137.
35. Gupta, R. A., and Dubois, R. N. (2001) Colorectal cancer prevention and treatment by inhibition of cyclooxygenase-2, *Nat. Rev. Cancer 1*, 11−21.
36. Grosch, S., Tegeder, I., Niederberger, E., Brautigam, L., and Geisslinger, G. (2001) COX-2 independent induction of cell cycle arrest and apoptosis in colon cancer cells by the selective COX-2 inhibitor celecoxib, *FASEB J. 15*, 2742−2744.
37. Zhang, X., Morham, S. G., Langenbach, R., and Young, D. A. (1999) Malignant transformation and antineoplastic actions of nonsteroidal antiinflammatory drugs (NSAIDs) on cyclooxygenase-null embryo fibroblasts, *J. Exp. Med. 190*, 451−459.
38. Wechter, W. J., Kantoci, D., Murray, E. D., Jr., Quiggle, D. D., Leipold, D. D., Gibson, K. M., and McCracken, J. D. (1997) R-Flurbiprofen chemoprevention and treatment of intestinal adenomas in the APC(Min)/+ mouse model: Implications for prophylaxis and treatment of colon cancer, *Cancer Res. 57*, 4316−4324.
39. Wechter, W. J., Leipold, D. D., Murray, E. D., Jr., Quiggle, D., McCracken, J. D., Barrios, R. S., and Greenberg, N. M. (2000) E-7869 (R-flurbiprofen) inhibits progression of prostate cancer in the TRAMP mouse, *Cancer Res. 60*, 2203−2208.
40. Kasum, C. M., Blair, C. K., Folsom, A. R., and Ross, J. A. (2003) Non-steroidal anti-inflammatory drug use and risk of adult leukemia, *Cancer Epidemiol. Biomarkers Prev. 12*, 534−537.
41. Mills, K. I., Gilkes, A. F., Sweeney, M., Choudhry, M. A., Woodgate, L. J., Bunce, C. M., Brown, G., and Burnett, A. K. (1998) Identification of a retinoic acid responsive aldoketoreductase expressed in HL60 leukaemic cells, *FEBS Lett. 440*, 158−162.
42. Bunce, C. M., Mountford, J. C., French, P. J., Mole, D. J., Durham, J., Michell, R. H., and Brown, G. (1996) Potentiation of myeloid differentiation by anti-inflammatory agents, by steroids and by retinoic acid involves a single intracellular target, probably an enzyme of the aldoketoreductase family, *Biochim. Biophys. Acta 1311*, 189−198.
43. Desmond, J. C., Mountford, J. C., Drayson, M. T., Walker, E. A., Hewison, M., Ride, J. P., Luong, Q. T., Hayden, R. E., Vanin, E. F., and Bunce, C. M. (2003) The aldo-keto reductase AKR1C3 is a novel suppressor of cell differentiation that provides a plausible target for the non-cyclooxygenase-dependent antineoplastic actions of nonsteroidal anti-inflammatory drugs, *Cancer Res. 63*, 505−512.
44. Lovering, A. L., Ride, J. P., Bunce, C. M., Desmond, J. C., Cummings, S. M., White, S. A. (2004) Crystal structures of prostaglandin D_2 11-ketoreductase (AKR1C3) in complex with the nonsteroidal anti-inflammatory drugs flufenamic acid and indomethacin, *Cancer Res. 64*, 1802−1810.
45. Matsuura, K., Shiraishi, H., Hara, A., Sato, K., Deyashiki, Y., Ninomiya, M., and Sakai, S. (1998) Identification of a principle mRNA species for human 3α-hydroxysteroid dehydrogenase isoform (AKR1C3) that exhibits high prostaglandin D_2 11-ketoreductase activity, *J. Biochem. 124*, 940−946.
46. Devane, W. A., Hanus, L., Breuer, A., Pertwee, R. G., Stevenson, L. A., Griffin, G., Gibson, D., Mandelbaum, A., Etinger, A., and Mechoulam, R. (1992) Isolation and structure of a brain constituent that binds to the cannabinoid receptor, *Science 258*, 1946−1949.
47. Cravatt, B. J., Prospero-Garcia, O., Siuzdak, G., Gilula, N. B., Henriksen, S. J., Boger, D. L., and Lerner, R. A. (1995) Chemical characterization of a family of brain lipids that induce sleep, *Science 268*, 1506−1509.
48. Sugiura, T., Kondo, S., Sukagawa, A., Nakane, S., Shinoda, A., Itoh, K., Yamashita, A., and Waku, K. (1995) 2-Arachidonylglycerol: A possible endogenous cannabinoid receptor ligand in brain, *Biochem. Biophys. Res. Commun. 215*, 89−97.
49. Yu, M., Ives, D., and Ramesha, C. S. (1997) Synthesis of prostaglandin E_2 ethanolamide from anandamide by cyclooxygenase-2, *J. Biol. Chem. 272*, 21181−21186.
50. Calignano, A., La Rana, G., Giuffrida, A., and Piomelli, D. (1998) Control of pain initiation by endogenous cannabinoids, *Nature 394*, 277−281.
51. Kozak, K. R., Rowlinson, S. W., and Marnett, L. J. (2000) Oxygenation of the endocannabinoid, 2-arachidonyl glycerol, to glyceryl prostaglandins by cyclooxygenase-2, *J. Biol. Chem. 275*, 33744−33749.
52. Kozak, K. R., Crews, B. C., Ray, J. L., Tai, H. H., Morrow, J. D., and Marnett, L. J. (2001) Metabolism of prostaglandin glycerol esters and prostaglandin ethanolamides in vitro and in vivo, *J. Biol. Chem. 276*, 36993−36998.
53. Berger, A., Crozier, G., Bisogno, T. J., Cavaliere, P., Innis, S., and Di Marzo, V. (2001) Anandamide and diet: Inclusion of dietary arachidonate and docosahexaenoate leads to increased brain levels of the corresponding *N*-acylethanolamines in piglets, *Proc. Natl. Acad. Sci. U.S.A. 98*, 6402−6406.
54. Hanus, L., Abu-Lafi, S., Fride, S., Breuer, A., Vogel, A., Shalev, D. E., Kustanovich, I., and Mechoulam, R. (2001) 2-Arachidonyl glyceryl ether, an endogenous agonist of the cannabinoid CB1 receptor, *Proc. Natl. Acad. Sci. U.S.A. 98*, 3662−3665.
55. Moody, J. S., Kozak, K. R., Ji, C., and Marnett, L. J. (2001) Selective oxygenation of the endocannabinoid 2-arachidonylglycerol by leukocyte-type 12-lipoxygenase, *Biochemistry 40*, 861−866.
56. Matias, I., Chen, J., De Petrocellis, L., Bisogno, T., Ligresti, A., Fezza, F., Krauss, A. H.-P., Shi, L., Protzman, C. E., Li, C., Liang, Y., Nieves, A. L., Kedzie, K. M., Burk, R. M., Di Marzo, V., and Woodward, D. F. (2004) Prostaglandin ethanolamides (prostamides): In vitro pharmacology and metabolism, *J. Pharmacol. Exp. Ther. 309*, 745−757.
57. Liang, Y., Li, C., Guzman, V. M., Evinger, A. J., III, Protzman, C. E., Krauss, A. H., and Woodward, D. F. (2003) Comparison of prostaglandin $F_{2\alpha}$, bimatoprost (prostamide), and butaprost (EP_2 agonist) on Cyr61 and connective tissue growth factor gene expression, *J. Biol. Chem. 278*, 27267−27277.
58. Higginbotham, E. J., Schuman, J. S., Goldberg, I., Gross, R. L., Van den Burgh, A. M., Chen, K., and Whitcup, S. M. (2002) One-year, randomized study comparing bimatoprost and timolol in glaucoma and ocular hypotension, *Arch. Ophthalmol. 120*, 1286−1293.
59. Noecker, R. S., Dirks, M. S., Choplin, N. T., Bernstein, P., Batoosingh, A. L., and Whitcup, S. M. (2003) A six-month randomized clinical trial comparing the IOP-lowering efficacy of Bimatoprost and Latanoprost in patients with ocular hypertension or glaucoma, *Am. J. Ophthalmol. 135*, 55−63.
60. Camras, C. B., Toris, C. B., Sjoquist, B., Milleson, M., Thorngren, J. O., Hejkal, T. W., Patel, N., Barnett, E. M., Smolyak, R., Hasan, S. F., Hellman, C., Meza, J. L., Wax, M. B., and Stjernschantz, J. (2004) Detection of the free acid of bimatoprost in aqueous humor samples from human eyes treated with bimatoprost before cataract surgery, *Ophthalmology 111*, 2193−2198.
61. Woodward, D. F., Krauss, A. H.-P., Chen, J., Liang, Y., Li, C., Protzman, C. E., Bogardus, A., Chen, R., Kedzie, K. M., Krauss, H. A.-P., Gil, D. W., Kharlamb, A., Wheeler, L. A., Babusis, D., Welty, D., Tang-Liu, D. D., Cherukury, M., Andrews, S. W., Burk, R. M., and Garst, M. E. (2003) Pharmacological characterization of a novel antiglaucoma agent, Bimatoprost (AGN 192024), *J. Pharmacol. Exp. Ther. 305*, 772−785.

62. Koda, N., Tsutsui, Y., Niwa, H., Ito, S., Woodward, D. F., and Watanabe, K. (2004) Synthesis of prostaglandin F ethanolamide by prostaglandin F synthase and identification of Bimatoprost as a potent inhibitor of the enzyme: New enzyme assay method using LC/ESI/MS, *Arch. Biochem. Biophys. 424*, 128−136.
63. Suzuki-Yamamoto, T., Nishizawa, M., Fukui, M., Okuda-Ashitaka, E., Nakajima, T., Ito, S., and Watanabe, K. (1999) cDNA cloning, expression and characterization of human prostaglandin F synthase, *FEBS Lett. 462*, 335−340.
64. Otwinowski, Z., and Minor, W. (1997) Processing of X-ray diffraction data collected in oscillation mode, *Methods Enzymol. 276*, 307−326.
65. Brünger, A. T. (1993) *X-PLOR 3.82: A system for X-ray crystallography and NMR*, Yale University Press, New Haven, CT.
66. Kunkel, T. A., Roberts, J. D., and Zakour, R. A. (1987) Rapid and efficient site-specific mutagenesis without phenotypic selection, *Methods Enzymol. 154*, 367−382.
67. Sanger, F., Nicklen, S., and Coulson, A. R. (1977) DNA sequencing with chain-terminating inhibitors, *Proc. Natl. Acad. Sci. U.S.A. 74*, 5463−5467.
68. Laskowski, R. A., MacArthur, M. W., Moss, D. S., and Thornton, J. M. (1993) ROCHECK: A program to check the stereochemical quality of protein structures, *J. Appl. Crystallogr. 26*, 283−291.
69. Jez, J. M., Bennett, M. J., Schlegel, B. P., Lewis, M., and Penning, T. M. (1997) Comparative anatomy of the aldo-keto reductase superfamily, *Biochem. J. 326*, 625−636.

BI051861T